



A Spatial Scan Statistic for Stochastic Scan Partitions

Author(s): Carey E. Priebe, Tim Olson, Dennis M. Healy, Jr.

Source: *Journal of the American Statistical Association*, Vol. 92, No. 440 (Dec., 1997), pp. 1476-1484

Published by: [American Statistical Association](#)

Stable URL: <http://www.jstor.org/stable/2965418>

Accessed: 09/12/2010 13:40

Your use of the JSTOR archive indicates your acceptance of JSTOR's Terms and Conditions of Use, available at <http://www.jstor.org/page/info/about/policies/terms.jsp>. JSTOR's Terms and Conditions of Use provides, in part, that unless you have obtained prior permission, you may not download an entire issue of a journal or multiple copies of articles, and you may use content in the JSTOR archive only for your personal, non-commercial use.

Please contact the publisher regarding any further use of this work. Publisher contact information may be obtained at <http://www.jstor.org/action/showPublisher?publisherCode=astata>.

Each copy of any part of a JSTOR transmission must contain the same copyright notice that appears on the screen or printed page of such transmission.

JSTOR is a not-for-profit service that helps scholars, researchers, and students discover, use, and build upon a wide range of content in a trusted digital archive. We use information technology and tools to increase productivity and facilitate new forms of scholarship. For more information about JSTOR, please contact support@jstor.org.



American Statistical Association is collaborating with JSTOR to digitize, preserve and extend access to *Journal of the American Statistical Association*.

<http://www.jstor.org>

A Spatial Scan Statistic for Stochastic Scan Partitions

Carey E. PRIEBE, Tim OLSON, and Dennis M. HEALY, Jr.

This article develops a spatial scan statistic for homogeneity analysis of point processes that utilizes stochastic scan partitions. The derivation of the sampling distribution for the statistic yields an exact test. This test has the potential for improved power over conventional alternatives when the point process is embedded in an underlying continuous random field and is recommended in situations for which the location of subregions of nonhomogeneity in the point process correspond to regions in the underlying field that can be segmented as distinct from their surroundings. The application to the detection of clustered microcalcifications in digital mammography is investigated as a motivating example.

KEY WORDS: Cluster detection; Digital mammography; Homogeneity; Image analysis; Poisson dispersion; Random field.

1. INTRODUCTION

In many situations one wishes to perform an analysis of the homogeneity of a point process. Testing for homogeneity against a clustering alternative is relevant in applications as diverse as astronomy (Cressie 1993), minefield detection (Muise and Smith 1992; Smith 1991), and regional disease mapping (Jacquez 1993). The example considered throughout this article is the detection of clustered microcalcifications in digital X-ray mammography.

Spiculated lesions, circumscribed masses, and clustered microcalcifications are among the important early indicators of malignant breast cancer, and early detection has been shown to improve survivability. Thus the detection of clustered microcalcifications in screening mammograms is an area of considerable research activity in the computer-aided detection and diagnosis community. The proceedings from the first three international workshops on digital mammography include results from numerous research efforts on this application, wherein homogeneity may imply the “uniformly healthy tissue” case and regions of nonhomogeneity warrant closer inspection (Bowyer and Astley 1994; Doi, Giger, Nishikawa, and Schmidt 1996; Gale, Astley, Dance, and Cairns 1994).

Consider a point process $\xi: I^d \rightarrow \{0, 1\}$ defined on I^d , the d -dimensional unit cube. The goal is to perform a Poisson dispersion test of $H_0: \text{Poisson}(\lambda)$ for λ fixed and known (*homogeneity*) versus the alternative that I^d is partitioned into disjoint regions R^0 and R^A and the point process is $\text{Poisson}(\lambda)$ on R^0 and $\text{Poisson}(\lambda' > \lambda)$ on R^A (*nonhomogeneity*). An intuitive approach to testing these hypotheses involves the quadrat counts of Fisher, Thornton, and Mackenzie (1922) (see Diggle 1983). The generalization to spatial scan statistics was considered by Adler (1984), Loader (1991), and Naus (1965), and more re-

cently by Alm (1997), Chen and Glaz (1996), and Kulldorff (1997). Analysis of the univariate scan process ($d = 1$) has been considered by many authors, including Cressie (1977, 1980), Loader (1991), and Naus (1965). As noted by Cressie (1993), exact results for $d \geq 2$ have proven elusive. This article considers a version of the scan process using *stochastic* and *disjoint* scan regions and provides an exact distribution under the null hypothesis of homogeneity.

The test presented here promises improved performance over conventional approaches under conditions found in several important application areas. Specifically, we note higher power when the point process is embedded in an underlying continuous random field $\zeta: I^d \rightarrow \mathfrak{R}$, as is the case in conventional gray-scale imagery, and when there is a correlation between R^A , the location of the anomalous subregion in the point process $\xi(x)$, and subregions of homogeneity in ζ . For example, in the simplest and best-case scenario, ζ^0 and ζ^A are strictly stationary and ergodic fields and $\zeta(x) = \zeta^0(x)\chi_{R^0}(x) + \zeta^A(x)\chi_{R^A}(x)$, where $\chi_R(x)$ is the indicator function for the set R .

As an example of the type of application for which higher power can be expected, we consider the case of gray-scale imagery in general and the detection of microcalcifications in digital mammography in particular. Given an image $\zeta(x)$, a realization of a continuous random field, two algorithms must be applied before performing the test for homogeneity. A detector $C(\zeta)$ is used to find microcalcifications, and a segmentation algorithm $W(\zeta)$ partitions I^d .

The first step is to obtain a detection map—a realization $\xi(x)$ of the point process. One simple example of such a detector is a matched filter (Castleman 1996; Jain 1989). Let $\hat{C}_\mu: \{\text{random fields on } I^d\} \rightarrow \{\text{random fields on } I^d\}$ be a matched (correlation) filter, where $\mu(x)$ is the generalized target signal against which the correlation is performed, such as a prototypical microcalcification; that is, $\hat{C}_\mu(\zeta)(x) = \int_{I^d} \zeta(z)\mu(z-x)dz$. A subset of the local maxima of this field is considered detections; the point process is obtained via $C(\zeta) = C_\mu(\zeta) = \chi_{\{\hat{C}'_\mu(x)=0 \text{ and } \lambda_{\max}(x) \leq \delta < 0\}}(x) = \xi(x)$, where $\lambda_{\max}(x)$ is the largest eigenvalue of $\hat{C}''_\mu(x)$ and δ is a threshold. Thus C :

Cary E. Priebe is Assistant Professor, Department of Mathematical Sciences, Johns Hopkins University, Baltimore, MD 21218. Tim Olson is Assistant Professor, Department of Mathematics, University of Florida, Gainesville, FL 32611. Dennis M. Healy, Jr. is Associate Professor, Departments of Mathematics and Computer Science, Dartmouth College, Hanover, NH 03755. This work was partially supported by Office of Naval Research grant N00014-95-1-0777, Office of Naval Research Grant N00004-96-1-0313, and Advanced Research Projects Agency as administered by the Air Force Office of Scientific Research under contract DOD F4960-93-1-0567. The authors thank the editor, an associate editor, and two anonymous referees for helpful comments that improved this article.

$\{\text{random fields on } I^d\} \rightarrow \{\text{point processes on } I^d\}$. The purpose of the dynamic thresholding is to produce a detection algorithm that yields a $\text{Poisson}(\lambda)$ detection map (with λ the intensity, or rate, of the uniformly distributed false positives) under the null hypotheses of no microcalcifications present with a high probability of detection in the presence of microcalcifications.

We also require a segmentation, or partitioning, algorithm $W: \{\text{random fields on } I^d\} \rightarrow \{\text{random partitions of } I^d\}$. Consider, for example, the watershed algorithm from mathematical morphology (Serra 1982; Vincent and Soille 1991). Although care must be taken to avoid ambiguity present in the geographical definition of watershed basins as the basins of attraction for the local minima of the realization ζ (Serra 1982, pp. 445–450), an intuitive idea of the algorithm can be based on the analogy to this physical example: Considering ζ as a surface in 3-space, the segmentation regions R_1, \dots, R_K are the “wells” defined by surrounding ridges, summits, and divides. Vincent and Soille (1991) gave an efficient algorithm for computing watersheds in digital gray-scale images.

Derivation of the exact sampling distribution under the null hypothesis for our test statistic requires the assumption of independence of the point process $\xi(x) = C(\zeta)$ and the stochastic partition $\{R_1, \dots, R_K\} = W(\zeta)$. We do not claim that this independence holds in general for all random fields ζ . Our example considers fields in specific application domains such as mammographic imagery. A useful (simplistic) model for the “white dots” in these images under the null hypothesis of no microcalcifications—for example, blood vessels imaged end-on—is “smooth, except for superimposed speckle.” The independence assumption in this situation is plausible in light of the spatial Fourier representation of the detection and segmentation operators; note that $C(\zeta)$ is a function of the high-frequency components of ζ , whereas $W(\zeta)$ is a function of the low-frequency components of ζ . Consider the simplest case, in which $C(\cdot)$ is a matched filter correlating with “single pixel white dots.” For the examples considered in this article, application of the watershed algorithm for determining the stochastic partition includes pre-smoothing with a median filter $P_\sigma(\cdot)$, where σ is the filter radius. The resultant partition $W_\sigma(\zeta) = W(P_\sigma(\zeta))$ thus inherits the robustness property of the median filter—the high breakdown point—in the sense that single pixel anomalies of the kind that determine the point process ξ have no effect (in the limit as the image resolution, and hence the number of pixels within the filter radius, increases) on the stochastic partition. Even though both the point process and the stochastic partition are obtained deterministically from the same field ζ , they are independent. This argument can be extended to matched filters correlating with any bounded target signal by increasing the radius σ of the median filter for larger target signals. This independence assumption is key to the derivation in Section 2.2 of the sampling distribution of the spatial scan statistic based on the stochastic partition. The

effect of this presmoothing on the partition $W_\sigma(\zeta)$ is investigated in Section 3.1.

In summary, given a realization ζ , $W(\zeta) = \{R_1, \dots, R_K\}$ produces a realized partition of I^d and $C(\zeta) = \xi$ yields a realized point process on I^d . The aforementioned proceedings of the international workshops on digital mammography contain numerous examples of microcalcification detection algorithms, by no means limited to matched filters; nonetheless, this detector provides a simple and sufficient example. Similarly, the literature contains many and varied mammogram segmentation algorithms based on methodologies quite different than watershed morphology; the first criterion for this choice is simplicity of a concrete example for the partitioning algorithm. In addition, derivation of the sampling distribution for the test statistic requires distributional information for the stochastic R_k , as discussed in Section 2, and the claim of higher power as compared to the conventional scan statistic requires $R^A \approx R_{k'}$ for some k' under H_A when $W(\zeta(x)) = W(\zeta^0(x)\chi_{R^0}(x) + \zeta^A(x)\chi_{R^A}(x))$.

In Section 2 we develop the spatial scan test for clustering based on stochastic partitions and discuss its power characteristics. In Section 3 we provide an example indicating that the assumptions made in deriving the test statistic are reasonable, a simulation example indicating the framework in which the test excels, and an example from digital mammography in which the test is recommended. In Section 4 we conclude with a discussion of relevance and extensions.

2. CLUSTER DETECTION USING STOCHASTIC PARTITIONS

2.1 Conventional Scan Statistics

Let $\xi: I^d \rightarrow \{0, 1\}$ denote a point process, with events occurring at spatial locations $x \in D \subset I^d$, where D is a random set. For $\delta > 0$, define the *scan process* as

$$\psi(x) = g(\{\xi(y) : y \in R(x, \delta)\}) \equiv g(R(x)),$$

defined for all $x \in \{y \in I^d : R(y, \delta) \subset I^d\}$. The $R(x, \delta)$ are *scan regions* about the spatial locations x , and $g(\cdot)$ denotes a function of the observations in a local neighborhood about x . The function g is termed the *locality statistic*. A standard choice for the scan regions and the locality statistic are d -dimensional cubes,

$$R(x, 2\delta) = \{y : x_j - \delta < y_j \leq x_j + \delta \text{ for } j = 1, \dots, d\},$$

and the number of events in the scan region,

$$g(R) = \text{cardinality}(D \cap R).$$

The *scan statistic* M maps the scan process to \mathfrak{R} . For the purpose of testing for nonhomogeneity as described here, a commonly used scan statistic is the maximum number of events in a region,

$$M = \max_{\text{regions } R} \{g(R)\}.$$

2.2 Testing Based on Stochastic Partitions

Let I^d be stochastically partitioned into K disjoint scan

regions, $I^d = \cup_{k=1}^K R_k$. That is, when the underlying field ζ is segmented, the segmentation regions R_k are stochastic, depending on the particular realization encountered. For instance, when the application involves detection of clusters of microcalcifications in mammographic images, the images are first segmented into local regions based on tissue texture.

Let the random variable M , the scan statistic, be defined as $M \equiv \max(N'_1, \dots, N'_K)$, where the locality statistics $N'_k = (N_k - \lambda t_k) / \sqrt{\lambda t_k}$ denote the standardized number of events N_k in region R_k and the t_k denote the spatial size of regions $R_k, t_k = |R_k|$. The t_k live on the simplex $S_K = \{(t_1, \dots, t_K) | t_k > 0 \text{ for all } k, \sum_{k=1}^K t_k = 1\}$.

The test rejects for large values of M . Under the null hypothesis that the point process is spatially homogeneous Poisson(λ) and $\xi(x)$ is independent of the partition $W(\zeta)$, the conditional cumulative distribution function for M is given by

$$\begin{aligned}
 F_M(m; \lambda, K | t_1, \dots, t_K) &= P_0(M \leq m | \lambda, K, t_1, \dots, t_K) \\
 &= e^{-\lambda} \prod_{k=1}^K \sum_{j=0}^{\lfloor m\sqrt{\lambda t_k} + \lambda t_k \rfloor} \frac{(\lambda t_k)^j}{j!}. \tag{1}
 \end{aligned}$$

Obtaining the desired unconditional distribution requires knowledge of the joint distribution of t_1, \dots, t_K . Assuming that $\zeta(x)$ is homogeneous under $H_0, W(\cdot)$ randomly partitions unit d volume. David (1970, pp. 79–82) considered the random partition of the unit interval into K subintervals using order statistics. Given X_i iid G ($i = 1, \dots, K - 1$) for continuous distribution G on $[0, 1]$, define G spacings as the lengths of the subintervals $Y_i = X_{(i)} - X_{(i-1)}$, where $X_{(0)} \equiv 0$. For $G = \text{uniform}(0, 1)$, the Y_i are said to be distributed as *uniform spacings*, identically distributed with joint density $(K - 1)!$ over $\bar{S}_{K-1} = \{(t_1, \dots, t_{K-1}) | t_k > 0 \text{ for all } k, \sum_{k=1}^{K-1} t_k \leq 1\}$. Distribution theory for more general G spacings was considered by Pyke (1965). For our present purpose, the region sizes t_1, \dots, t_{K-1} , with $t_K = 1 - \sum_{k=1}^{K-1} t_k$, play the role of the Y_i , partitioning unit volume. Under H_0 , they are indeed identically distributed. In view of the probability integral transformation, a particularly relevant choice of $F_{t_1, \dots, t_{K-1}}$ is uniform spacings. We have the following result, proved using combinatorics and multivariable calculus (see the Appendix).

Theorem. Let the t_k be distributed as uniform spacings. Then the sampling distribution for the scan statistic M under the null hypothesis is given by the cumulative distribution function

$$\begin{aligned}
 F_M(m; \lambda, K) &= \int F_M(m; \lambda, K | t_1, \dots, t_K) dF_{t_1, \dots, t_{K-1}} \\
 &= e^{-\lambda} (K - 1)! \int_{\bar{S}_{K-1}} \prod_{k=1}^K \sum_{j=0}^{\lfloor m\sqrt{\lambda t_k} + \lambda t_k \rfloor} \frac{(\lambda t_k)^j}{j!} d\bar{S}_{K-1}
 \end{aligned}$$

$$\begin{aligned}
 &= e^{-\lambda} (K - 1)! \sum_{j_1=0}^C \dots \sum_{j_K=0}^C \lambda^{\sum_{k=1}^K j_k} \left(\prod_{k=1}^K j_k! \right)^{-1} \\
 &\quad \times s^{K-1} \sum_{i=0}^{j_K} \frac{j_K!}{i!} a_{j_K}^i s^{j_K-i} \\
 &\quad \times \sum_{l_1=0}^{j_1} \dots \sum_{l_{K-1}=0}^{j_{K-1}} \prod_{k=1}^{K-1} \frac{j_k!}{(j_k - l_k)!} s^{l_k} a_{j_k}^{j_k-l_k} \\
 &\quad \times \frac{1}{\left(\sum_{k=1}^{K-1} l_k + j_K - i + K - 1 \right)!}, \tag{2}
 \end{aligned}$$

where $\lfloor x \rfloor$ represents the floor of $x, C = \lfloor m\sqrt{\lambda} + \lambda \rfloor, a_{j_k} = (m^2 + 2j_k - m\sqrt{m^2 + 4j_k}) / (2\lambda)$, and $s = s(j_1, \dots, j_K) = 1 - \sum_{k=1}^K a_{j_k}$.

2.3 Comments

We present some points of discussion concerning the test that we have developed.

1. Calculation of $1 - F_M(m_{\text{observed}} - 1; \lambda, K)$ given in (2) yields an exact p -value for the test of homogeneity.

2. Equation (1) characterizes a *restricted Poisson dispersion* likelihood ratio test statistic with unequal sample sizes. Rejecting for large values of M is equivalent to a generalized likelihood ratio test, rejecting for large $\max(Z_1, \dots, Z_K)$, where $Z_k = 2((\lambda t_k - N_k) + N_k \log(N_k / \lambda t_k))$, when the partition $\{R_k\}$ is assumed to correspond to the alternative hypothesis partition $\{R^0, R^A\}$ in the sense that $R^A \subset R_k$ for some k .

3. The assumption of uniform spacings for the t_k under the null hypothesis seems plausible for the particular partitioning algorithm $W(\cdot)$ considered in later examples, the watershed algorithm. An empirical investigation of this assumption is presented in Section 3, Example 1.

4. An approximation for $F_M(m; \lambda, K)$ is useful for large m, λ, K as the complexity of (2) is polynomial in λ and exponential in K . Writing $h(t) = \sum_{j=0}^{\lfloor m\sqrt{\lambda t} + \lambda t \rfloor} \{(\lambda t)^j / j!\}$, (2) yields

$$F_M(m; \lambda, K) = e^{-\lambda} (K - 1)! h * h * \dots * h(1), \tag{3}$$

the convolution of h with itself $K - 1$ times evaluated at unity. This convolution may be approximated efficiently using numerical Fourier transform algorithms.

5. A simple form for $F_M(m; \lambda)$ is also justifiable under the null hypothesis in some cases. Thus for stochastic K , we have

$$\begin{aligned}
 F_M(m; \lambda) &= \sum_{\kappa=2}^{\infty} f_K(\kappa) e^{-\lambda} (\kappa - 1)! \\
 &\quad \times \int_{\bar{S}_{\kappa-1}} \prod_{k=1}^{\kappa} \sum_{j=0}^{m(t_k)} \frac{(\lambda t_k)^j}{j!} d\bar{S}_{\kappa-1}, \tag{4}
 \end{aligned}$$

where $f_K(\kappa) = P(K = \kappa)$ is the probability that the stochastic partition is made up of $K = \kappa$ regions, $\kappa =$

2, 3, . . . ($\kappa = 1$ does not allow a test.) An investigation of this is provided in Section 3, Example 1.

2.4 The Power of the Test

The power of the test depends on the accuracy of the partition boundaries as estimates of “true” boundaries, the difference in intensities λ and λ' , and the size of the region of nonhomogeneity R^A . In the example considered herein, the stochastic partition involves segmenting the mammogram into local regions based on tissue texture. If microcalcification clusters are likely to be contained within a sub-region of tissue with texture different than the healthy tissue, then this partitioning scheme has the potential to yield greater power than a standard quadrat test or a conventional spatial scan statistic. The power of the test based on (2) can be calculated exactly. In particular, we consider the best-case scenario in which R^A is small relative to I^d and a single scan region corresponds to the region of nonhomogeneity, $R^A = R_{k'}$, for some k' . That is, for $W(\zeta) = W(\zeta^0(x)\chi_{R^0}(x) + \zeta^A(x)\chi_{R^A}(x)) \cong \{R^A, R_2, \dots, R_K\}$ under H_A , we have

$$\begin{aligned} \text{power}_\alpha &= P_A(M \geq m_\alpha) = 1 - P_A(M \leq m_\alpha - 1) \\ &= 1 - F_{\text{Poisson}(\lambda' t_{k'})}((m_\alpha - 1)\sqrt{\lambda t_{k'}} + \lambda t_{k'}) \\ &\quad \times \int_{\tilde{S}'_{K-2}} \prod_{k \neq k'} F_{\text{Poisson}(\lambda t_k)} \\ &\quad \times ((m_\alpha - 1)\sqrt{\lambda t_k} + \lambda t_k) d\tilde{S}'_{K-2}. \end{aligned} \tag{5}$$

The integral term can be calculated exactly, using the same technique as in the theorem, and is approximately $1 - \alpha$ for small $t_{k'} = t^A$. $\varepsilon(\lambda') = F_{\text{Poisson}(\lambda' t_{k'})}((m_\alpha - 1)\sqrt{\lambda t_{k'}} + \lambda t_{k'}) \rightarrow 0$ as $\lambda' \rightarrow \infty$. Thus $\text{power}_\alpha \rightarrow 1$ as $\lambda' \rightarrow \infty$, as expected. Compare this to the best-case scenario, in which the two regions R^0 and R^A are known. Then

$$\text{power}_{\text{optimal}} = 1 - \varepsilon(\lambda') F_{\text{Poisson}(\lambda t^0)}((m_\alpha - 1)\sqrt{\lambda t^0} + \lambda t^0). \tag{6}$$

The only way to obtain power approaching that given in (5) or (6) when using quadrats or conventional scan statistics is to guess correctly and have one scan region match R^A perfectly. For quadrats, this requires perfect knowledge of the size, shape, and location of R^A . Conventional scan statistics relieve the requirement for a priori location information, but traditionally use hyperrectangles of one or a few sizes and thus still require a fortuitous choice for the anticipated size and shape. In light of this analysis, it should not be surprising that (2) yields higher power, approaching (6), because we are in essence assuming that the information about R^A is available through the segmentation $W(\zeta)$.

When $R^A \subsetneq R_{k'}$, or when $R^A = R_{k'_1} \cup R_{k'_2}$, the power of (2) is reduced. In the first case this suboptimality is due to the decreased “effective intensity” observed in $R_{k'}$, proportional to the size of the region $R_{k'} \setminus R^A$ which has intensity λ rather than λ' . The latter segmentation causes the additional observed events in R^A to be split between $R_{k'_1}$ and $R_{k'_2}$, rather than being concentrated in a single $R_{k'}$, with a

resultant decrease in power for λ' large with respect to λ . Continuing the comparison with conventional scan statistics, note that the absence of size and shape information regarding R^A implies that one of these two suboptimality cases will hold. Although the power of the conventional scan statistic is higher than that of the quadrat approach with fixed partitions (Naus 1966), the method of stochastic partitions yields an improvement for “correct” partitions $\{R^A, R_2, \dots, R_K\}$.

The simulation and mammography examples in Section 3 provide insight into the power of the test in specific cases.

3. EXAMPLES

This section presents an example indicating that the assumptions made in deriving the test statistic are reasonable, at least for the digital mammography application, a simulation example indicating the framework in which the test provides improved power over alternatives, and an example of test performance in digital mammography.

3.1 Example 1: Investigation of Uniform Spacings Assumption

The first example, an empirical investigation of the assumption of uniform spacing for the t_k under the null hypothesis, is presented in Figures 1 and 2. Consider an image $\zeta(x)$; for example, a digitized mammogram. The watershed algorithm $W(\zeta)$ yields the scan regions R_k . We consider the chi-squared Pearson and the Kolmogorov–Smirnov (K–S) tests of the marginal distribution of the region sizes t_k versus the uniform spacings distribution. Following David (1970), we have

$$\begin{aligned} f_{t_k}(u) &= \text{beta}(u; 1, K - 1) \\ &= (K - 1)(1 - u)^{K-2} \quad \text{for } 0 \leq u \leq 1, \end{aligned}$$

and the marginal distribution is the incomplete beta function $F_{t_k}(a) = \int_0^a f_{t_k}(u) du = I_a(1, K - 1)$ for $0 \leq a \leq 1$. Figure 1 gives the results of running the watershed algorithm on a healthy mammogram, comparing the empirical and theoretical cdfs (Fig. 1c). Both the chi-squared and K–S tests convincingly fail to reject the uniform spacings hypothesis.

The number of watershed regions K —the number of local minima—is a measure of the “roughness” of the image ζ , and thus can be controlled somewhat by presmoothing. Let $P_\sigma(\cdot)$ be a median filter with smoothing parameter (filter radius) σ . Figure 2 represents the results of performing the same test procedure described for Figure 1 for a set of 49 healthy mammograms. The partitions are obtained via $W(P_\sigma(\zeta))$ for six different settings of σ . We thus present six K–S p values for each mammogram. Except for perhaps $\sigma = 1$, which produces the most regions (the median number of regions ranges from $\hat{\mu}_{K_1} = 172.9$ for $\sigma = 1$ to $\hat{\mu}_{K_6} = 18.1$ for $\sigma = 6$ for these 256×256 pixel images), we find no deviation from what would be expected under the uniform spacings hypothesis. We conclude that the assumption of uniform spacings under the null hypothesis made in the theorem for the watershed algorithm as applied to digital mammography is reasonable. The results

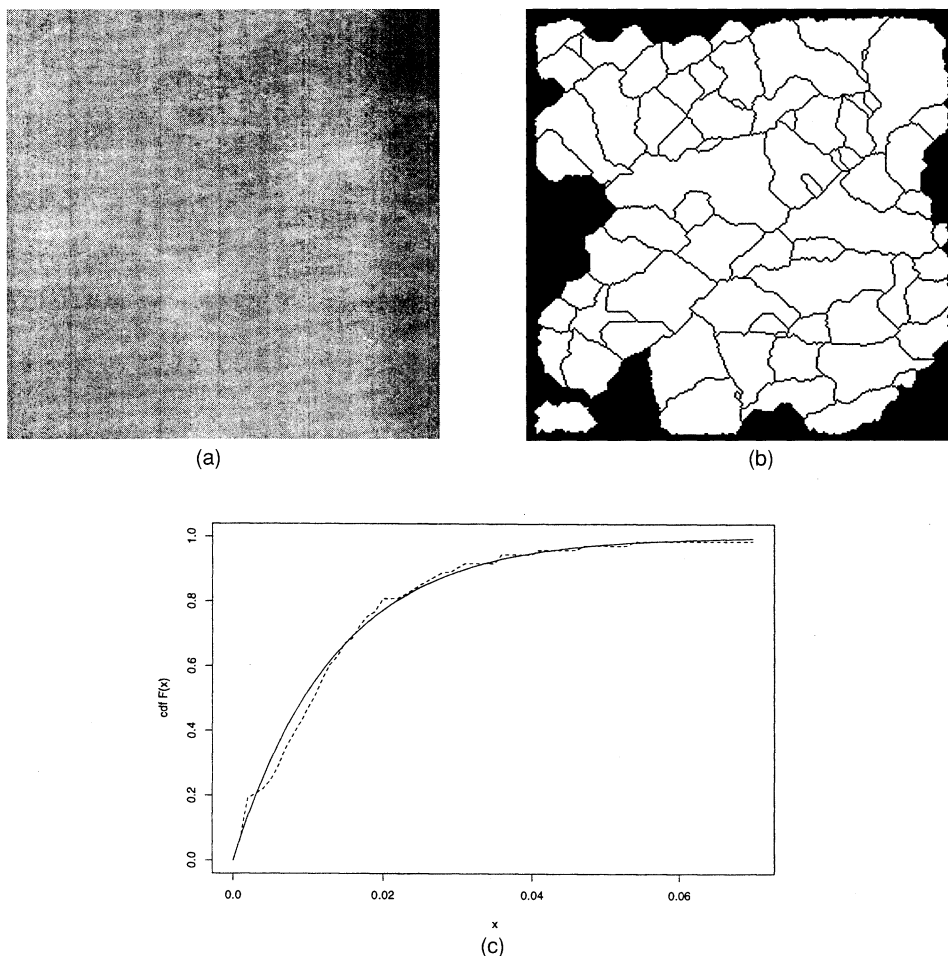


Figure 1. Investigation of the Uniform Spacings Assumption. Panel (a) depicts a homogeneous (healthy) mammogram. Panel (b) depicts the watershed regions. Panel (c) compares the empirical and theoretical cdfs. [—, beta(1, 72); ---, empirical]. The Kolmogorov–Smirnov p value for a test of the spacing distribution for the marginal of watershed region sizes is .58. The chi-squared p value is .34. We cannot reject the null hypothesis. Figure 2 indicates that this result generalizes.

of this experiment seem plausible, from an investigation of the statistical properties of the watershed algorithm.

The aforementioned experiment also provides an exam-

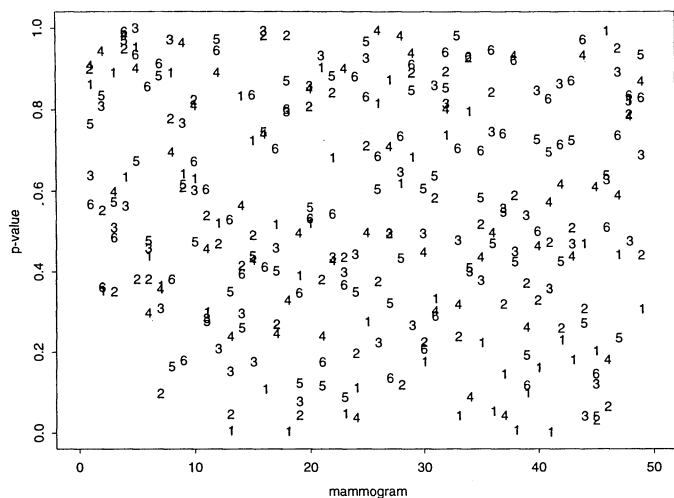


Figure 2. Analysis of the Spacings Hypothesis for the Marginal Size Distribution. K–S p values for a test of the uniform spacings distribution for the marginal of watershed region sizes. The data are a set of 49 healthy mammograms. For each image, six different presmoothing settings for the watershed algorithm are used. The p values appear uniformly distributed, as would be expected under the null hypothesis.

ple of a sample from $f_K(\kappa) = P(K = \kappa)$, presented in Figure 3. Corresponding to smoothing with $\sigma = 3$ from Figure 2 and having a median number of regions $\hat{\mu}_{K_3} = 54.9$ over the 49 healthy mammograms, Figure 3 indicates both graphically and via tests of normality that hypothesizing a multinomial approximation to a normal distribution for $f_K(\kappa)$ may indeed be reasonable in obtaining (4).

3.2 Example 2: Simulated Example

Figure 4 considers a simulated example of using (3) to test for homogeneity. The nonhomogeneous process considered here mirrors that of Muise and Smith (1992) for minefield simulations. A homogeneous Poisson (λ) process is generated in I^2 (Fig. 4a); and a corresponding nonhomogeneous process is generated in I^2 by adding another Poisson($\lambda' > \lambda$) process generated in R^A (Fig. 4b). For this example $\lambda = 20$, $\lambda' = 270$, $R^A = [.2, .4] \times [.2, .4]$, $|R^A| = t^A = 1/25$, and $R^0 = I^2 \setminus R^A$. (Example interpretation: We expect approximately 20 false microcalcification detections in the mammogram; a small region—4% of the total image size—has a cluster of microcalcifications that will produce approximately 10 detections.) These point processes are considered to be embedded in simulated random fields, and the watershed algorithm is applied to these fields. The

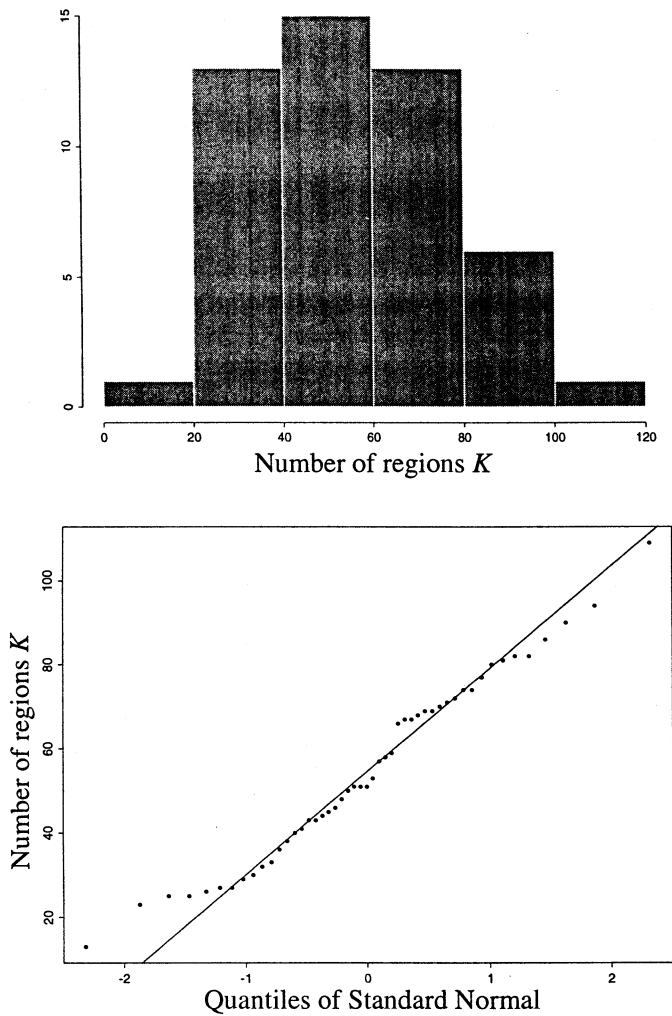


Figure 3. Analysis of the Number of Regions K Produced by the Watershed Algorithm Applied to Healthy Mammograms. The estimate of $f_K(\kappa) = P(P = \kappa)$ is based on the set of 49 healthy mammograms, using smoothing parameter $\sigma = 3$. The K-S p value versus normality is .244; the chi-squared p value versus normality is .912. It may be reasonable to hypothesize a multinomial approximation to a normal distribution for $f_K(\kappa)$.

field corresponding to the homogeneous process is homogeneous as well, yielding the watershed scan regions depicted in Figure 4c. The field corresponding to the nonhomogeneous process is nonhomogeneous, having different structure in the region R^A ; $\zeta(x) = \zeta^0(x)\chi_{R^0}(x) + \zeta^A(x)\chi_{R^A}(x)$, where ζ^0 and ζ^A have different distribution functions. Figure 4d shows the watershed scan regions for this case; ζ^0 and ζ^A have been chosen so that $W(\zeta) = W(\zeta^0(x)\chi_{R^0}(x) + \zeta^A(x)\chi_{R^A}(x)) \cong \{R^A, R_2, \dots, R_K\}$. In Figure 4c and 4d, the corresponding point process is overlaid.

For this example, we obtain the following results from (3):

Homogeneous process:

$$K = 24; \sum N_k = 16; M = 1.997; p \text{ value} = .52;$$

Nonhomogeneous process:

$$K = 24; \sum N_k = 27; M = 9.146; p \text{ value} = 0.$$

For comparison, the quadrats approach using 25 regions (also perfectly aligned, with one quadrat region = R^A) yields p values of .20 and 0 for the homogeneous and nonhomogeneous examples. Both approaches have been afforded best-case power characteristics due to the optimal alignment of one scan region with the region of nonhomogeneity R^A .

3.3 Monte Carlo Power Comparison

To buttress the results of the power analysis presented in Section 2.4, we now present a small study via Monte Carlo simulation providing formal numerical comparison of power characteristics with competing procedures. The simulation scenario is similar to that of the preceding example. A homogeneous Poisson($\lambda = 20$) process is generated in $R^0 = I^2 \setminus R^A$, and a corresponding process is generated in I^2 by combining with another Poisson(λ') process generated in R^A . For this simulation study, R^A is a $.2 \times .2$ square oriented with the coordinate axes and randomly located in I^2 . The value used for λ' ranges from 20 (homogeneity) to 270 (in which we expect 10 additional events in R^A). This point process is considered to be embedded in a simulated random field $\zeta(x) = \zeta^0(x)\chi_{R^0}(x) + \zeta^A(x)\chi_{R^A}(x)$. The watershed algorithm is applied to this field, producing $W(\zeta) \cong \{R^A, R_2, \dots, R_K\}$.

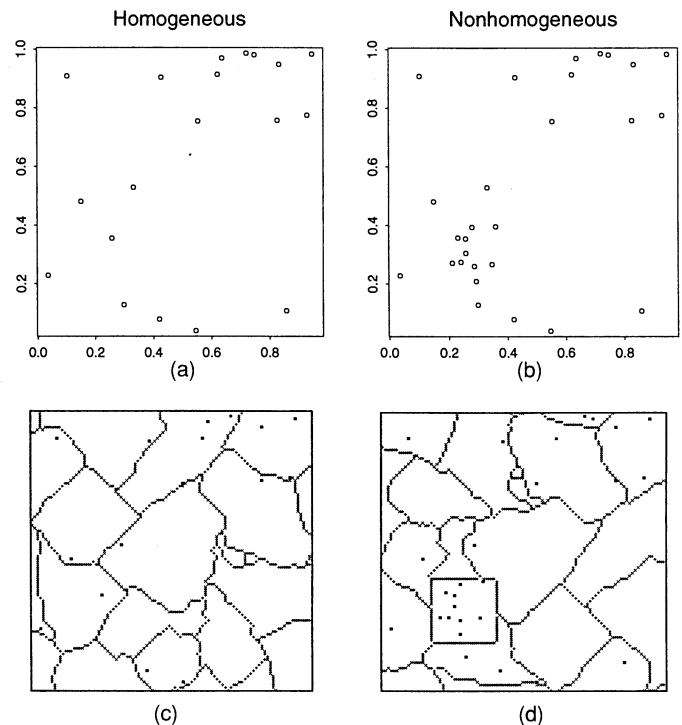


Figure 4. Simulated Example of Using Stochastic Scan Regions to Test for Homogeneity. Panel (a) depicts a homogeneous Poisson(λ) process in I^2 . Panel (b) depicts a nonhomogeneous process in I^2 that is Poisson(λ) in R^0 and Poisson($\lambda' > \lambda$) in R^A . $\lambda = 20$, $\lambda' = 270$, $R^A = [.2, .4] \times [.2, .4]$, $|R^A| = t^A = 1/25$, and $R^0 = I^2 \setminus R^A$. These processes are embedded in simulated random fields f^0 and f^A . The field f^0 is homogeneous, whereas f^A is nonhomogeneous, having a different distribution in R^A than in R^0 . The watershed algorithm is applied to these fields, yielding the scan regions depicted in panels (c) and (d). This example yields the following results: (homogeneous process) $K = 24$; $\sum N_k = 16$; $M = 1.997$; $p \text{ value} = .52$; (nonhomogeneous process) $K = 24$; $\sum N_k = 27$; $M = 9.146$; $p \text{ value} = 0$.

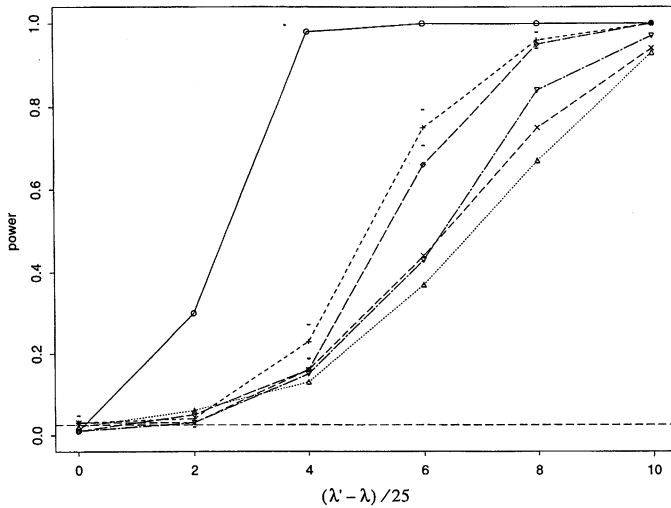


Figure 5. Power Curves From Monte Carlo Simulation in a Setting Analogous to that of Figure 4. Here 100 Monte Carlo replications were performed for various values of λ' . $(\lambda' - \lambda)/25$ represents the expected number of excess points in the randomly located $.2 \times .2$ square subregion R^A . The nominal level of the test is .025. The procedures compared include our method using stochastic scan partitions (SSP, denoted by +), the quadrat approach in which the size of the quadrats is chosen correctly (QUADRAT, denoted by Δ), the Chen and Glaz (1996) approximation for the conventional scan statistic (CG) with three choices for the size of the scan window—CG(.1 \times .1), denoted by \times ; CG(.2 \times .2), denoted by \diamond ; and CG(.4 \times .4), denoted by ∇ —and the “perfect knowledge” (OPTIMAL, denoted by \circ) case in which both the size and the location of the region of nonhomogeneity are known. For SSP, the partition is obtained by applying the watershed algorithm to a simulated random field $\zeta(x) = \zeta^0(x)\chi_{R^0}(x) + \zeta^A(x)\chi_{R^A}(x)$. Included in the figure are the approximate one-standard deviation bounds for our stochastic scan partition method. These curves indicate that when a partition approximating $\{R^A, R_2, \dots, R_K\}$ is obtained, our method can improve significantly upon the power of both the quadrat approach and the conventional scan statistic, except perhaps when the scan statistic uses the correct choice of scan window. These results agree with those of the theoretical analysis of Section 2.4.

The procedures compared include our method using stochastic scan partitions (SSP), the quadrat approach in which the size of the quadrats is chosen correctly (.2 \times .2), and the conventional scan statistic with three choices for the size of the scan window: too small (.1 \times .1), correct, and too large (.4 \times .4). Because the exact distribution of the conventional spatial scan statistic is not available, we make use of the approximation provided by Chen and Glaz (1996). We also include a comparison against the optimal “perfect knowledge” case in which both the size and the location of the region of nonhomogeneity is known.

Figure 5 presents the results of this simulation, in which 100 Monte Carlo replications were performed for each value of λ' , in the form of power curves. The nominal level of the test is set to be .025. (Randomization is required for all of the tests compared, except SSP, to achieve this nominal level.) Included in the figure are the approximate one standard deviation bounds for our stochastic scan partition method. These results show that when a partition approximating $\{R^A, R_2, \dots, R_K\}$ is obtained, our method can improve significantly on the power of both the quadrat approach and the conventional scan statistic, except perhaps when compared against the scan statistic using the correct choice of scan window. These results agree with those of

the theoretical analysis of Section 2.4 and indicate numerically the potential improvement to be gained by using the stochastic scan partitions method when the underlying random field provides information about the region of nonhomogeneity.

3.4 Example 3: Digital Mammography

In addition to the watershed segmentation algorithm, application of the test requires a detection algorithm that produces an appropriate point process. We use the variation of the standard matched filter $C(\cdot)$ described earlier and apply the procedure described in Example 2 to digitized mammograms.

Figure 6 depicts the results of applying the test (3) to digital mammography. The results indicate the advantage of utilizing scan regions obtained through a segmentation of the random field underlying the point process. For this example the watershed and matched filter algorithms were applied to two mammograms; one healthy and one (Fig. 6a), containing the cluster of microcalcifications seen in Figure 6b. For the healthy mammogram, (3) yields a p value of .98 (with 36 regions) and quadrats yield a p value of .97 (with 42 regions). For the nonhomogeneous mammogram, (3) yields a p value of .034 (with 44 regions) and quadrats yield a p value of .41 (with 42 regions). This improvement over the quadrats approach, a manifestation of the greater power of

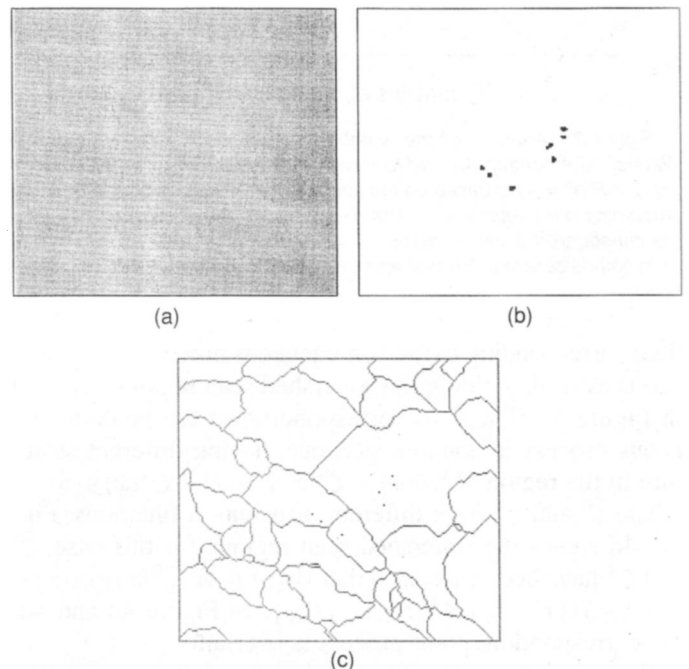


Figure 6. Testing the Homogeneity of Digital Mammographic Images. For a healthy mammogram, (3) yields a p value of .98 (with 36 regions) and quadrats yield a p value of .97 (with 42 regions). For the nonhomogeneous mammogram depicted in panel (a) containing the microcalcifications seen in panel (b), (3) yields a p value of .034 (with 44 regions) and quadrats yield a p value of .41 (with 42 regions). The superior power of the test given by (3) is due to the fact that a single watershed region contains the entire upper-right cluster of four microcalcifications, as seen in panel (c), whereas the quadrat regions split this cluster. The results indicate the advantage of utilizing scan regions obtained through a segmentation of the random field underlying the point process.

the test utilizing stochastic scan regions, is due to the fact that a single watershed region contains the entire upper-right cluster of four microcalcifications (Fig. 6c), whereas the quadrat regions split this cluster.

4. CONCLUSIONS

We have developed a spatial scan statistic for testing the homogeneity of a Poisson process against a clustering alternative. The approach utilizes stochastic and disjoint scan regions, and the exact distribution of the test statistic has been derived. We have compared this to simple approaches using quadrats as well as more sophisticated scan statistics that still require a priori choices for the sizes of the scan regions and for which only approximations are available. The test has the potential for improved power over these competing approaches when the point process is embedded in a general random field, as is the case for targets in images. Other approaches to testing the homogeneity of a spatial point process, such as point-to-point distance statistics, have not been considered.

The test has been developed for H_0 : Poisson(λ), λ fixed and known on I^d versus H_A : Poisson(λ) on R^0 and Poisson($\lambda' > \lambda$) on R^A , $R^0 \cup R^A = I^d$ and $R^0 \cap R^A = \emptyset$. The test is not constrained to two-dimensional processes, and the examples of both $C(\cdot)$ and $W(\cdot)$ presented earlier are easily generalized to higher-dimensional fields. In particular, point processes arising from volumetric brain imaging can be treated. An analogous derivation yields tests for binomial processes and for $\lambda' < \lambda$ and $\lambda' \neq \lambda$. For unknown λ , using the estimate $\hat{\lambda} = \sum N_k$ in (2) or (4) yields the appropriate test, with a degradation in power proportional to the size of region R^A . But in practice, λ often can be accurately estimated by performing a large number of tests. For example, a particular microcalcification detection algorithm can be applied to a set of healthy mammograms to determine the value of λ to be used under the null hypothesis.

In statistical image analysis applications, the utility of the test relies on the availability of a detection algorithm and a segmentation algorithm. We have used simple, well-known choices for these image-processing algorithms. The validity of the test requires knowledge of the stochastic behavior of the segmentation algorithm. Examples indicate that the watershed algorithm behaves as required under H_0 . The power of the test depends on the assumption that the point process and the field in which it is embedded are not independent of one another under the alternative hypothesis, and on the ability of the segmentation algorithm to localize regions in which the point process is likely to be homogeneous. For the detector, all Poisson dispersion tests require that the point process obtained be Poisson and homogeneous under H_0 . That is, the noise process is modeled as complete spatial randomness. Power depends on the ability to detect targets when they are present. We have used standard matched filter-type detection algorithms. It is clear that better detection and segmentation algorithms provide more reliable tests. Research and development in these two areas is ongoing in engineering and the mathematical sciences.

The test developed in this article is valid for any choice of algorithms meeting the foregoing conditions; our purpose has not been to optimize these algorithms, but rather to develop a test that incorporates the potential capabilities of a segmentation algorithm to produce appropriate stochastic partitions.

APPENDIX: PROOFS

Let $K \in \{2, 3, \dots\}$ regions partition I^d , with sizes t_k . ‘‘Uniform spacings’’ (David 1970) implies that t_1, \dots, t_{K-1} , with $t_K = 1 - \sum_{k=1}^{K-1} t_k$, are distributed with joint pdf $(K-1)!$ over

$$\bar{S}_{K-1} = \left\{ (t_1, \dots, t_{K-1}) \mid t_k > 0 \forall k, \sum_{k=1}^{K-1} t_k \leq 1 \right\}.$$

Let $\lambda \in \mathbb{R}^+$, $m \in [-\sqrt{\lambda}, \infty)$ and K be fixed, and let $c(t_k) = \lfloor m\sqrt{\lambda t_k} + \lambda t_k \rfloor$, where $\lfloor x \rfloor$ represents the floor of x . Theorem 1 is proved using nothing more than combinatorics and multivariable calculus. We require the following lemma, obtained via integration by parts and induction.

Lemma 1.

$$\int_{\bar{S}_{K-1}} \prod_{k=1}^K t_k^{j_k} d\bar{S}_{K-1} = \frac{\prod_{k=1}^K (j_k!)}{(\sum_{k=1}^K j_k + K - 1)!}.$$

We now proceed to the proof of Theorem 1.

Proof of Theorem 1

We have, under the null hypothesis,

$$\begin{aligned} F_M(m; \lambda, K) &= e^{-\lambda} (K-1)! \int_{\bar{S}_{K-1}} \prod_{k=1}^K \sum_{j=0}^{c(t_k)} \frac{(\lambda t_k)^j}{j!} d\bar{S}_{K-1} \\ &= e^{-\lambda} (K-1)! \int_{\bar{S}_{K-1}} \sum_{j_1=0}^{c(t_1)} \dots \sum_{j_K=0}^{c(t_K)} \prod_{k=1}^K \frac{(\lambda t_k)^{j_k}}{j_k!} d\bar{S}_{K-1}. \end{aligned}$$

The support of $t_k^{j_k}$ is $c(t_k) \geq j_k$. Solving the quadratic equation yields $(m^2 + 2j_k - m\sqrt{m^2 + 4j_k})/(2\lambda) \leq t_k \leq 1$. Writing $a_{j_k} = (m^2 + 2j_k - m\sqrt{m^2 + 4j_k})/(2\lambda)$ and letting $\chi_{[a,b]}(t)$ be the indicator function for the set $[a, b]$, define

$$\chi(a_{j_k}, t_k) = \chi_{[a_{j_k}, 1]}(t_k) = \begin{cases} 1 & \text{for } a_{j_k} \leq t_k \leq 1 \\ 0 & \text{otherwise,} \end{cases}$$

representing the support of $t_k^{j_k}$. Defining $C = c(1) = \lfloor m\sqrt{\lambda} + \lambda \rfloor$ yields

$$\begin{aligned} F_M(m; \lambda, K) &= e^{-\lambda} (K-1)! \int_{\bar{S}_{K-1}} \sum_{j_1=0}^C \dots \sum_{j_K=0}^C \prod_{k=1}^K \frac{(\lambda t_k)^{j_k}}{j_k!} \\ &\quad \times \chi(a_{j_k}, t_k) d\bar{S}_{K-1} \\ &= e^{-\lambda} (K-1)! \sum_{j_1=0}^C \dots \sum_{j_K=0}^C \lambda^{\sum_{k=1}^K j_k} \left(\prod_{k=1}^K j_k! \right)^{-1} \\ &\quad \times \int_{\bar{S}_{K-1}} \prod_{k=1}^K t_k^{j_k} \chi(a_{j_k}, t_k) d\bar{S}_{K-1}. \end{aligned}$$

It remains to integrate $I(j_1, \dots, j_K) = \int_{\bar{S}_{K-1}} \prod_{k=1}^K t_k^{j_k} \chi(a_{j_k}, t_k) d\bar{S}_{K-1}$. The simplex constraints give us $t_K = 1 - \sum_{k=1}^{K-1} t_k$, and so

$$\begin{aligned} I(j_1, \dots, j_K) &= \int_0^1 \int_0^{1-t_1} \dots \int_0^{1-\sum_{k=1}^{K-2} t_k} \left(\prod_{k=1}^{K-1} t_k^{j_k} \right) \left(1 - \sum_{k=1}^{K-1} t_k \right)^{j_K} \\ &\quad \times \left(\prod_{k=1}^{K-1} \chi(a_{j_k}, t_k) \right) \chi \left(a_{j_K}, 1 - \sum_{k=1}^{K-1} t_k \right) dt_1 \dots dt_{K-1} \\ &= \int_{a_{j_1}}^{1-\sum_{k=2}^K a_{j_k}} \int_{a_{j_2}}^{1-t_1-\sum_{k=3}^K a_{j_k}} \dots \int_{a_{j_{K-1}}}^{1-\sum_{k=1}^{K-2} t_k - a_{j_K}} \\ &\quad \times \left(\prod_{k=1}^{K-1} t_k^{j_k} \right) \left(1 - \sum_{k=1}^{K-1} t_k \right)^{j_K} dt_1 \dots dt_{K-1}. \end{aligned}$$

We address the foregoing integral via the change of variables $t_k = su_k + a_{j_k}$ for $0 \leq u_k \leq 1 - \sum_{l=1}^{k-1} u_l$, $k = 1, \dots, K-1$, and $s = s(j_1, \dots, j_K) = 1 - \sum_{k=1}^K a_{j_k}$, obtaining

$$\begin{aligned} I(j_1, \dots, j_K) &= s^{K-1} \int_0^1 \int_0^{1-u_1} \dots \int_0^{1-\sum_{k=1}^{K-2} u_k} \left(\prod_{k=1}^{K-1} (su_k + a_{j_k})^{j_k} \right) \\ &\quad \times \left(1 - \sum_{k=1}^{K-1} (su_k + a_{j_k}) \right)^{j_K} du_1 \dots du_{K-1} \\ &= s^{K-1} \sum_{i=0}^{j_K} \binom{j_K}{i} a_{j_K}^i s^{j_K-i} \sum_{l_1=0}^{j_1} \dots \sum_{l_{K-1}=0}^{j_{K-1}} \\ &\quad \times \left(\prod_{k=1}^{K-1} \binom{j_k}{l_k} s^{l_k} a_{j_k}^{j_k-l_k} \right) \\ &\quad \times \left(\frac{(j_K - i)! \prod_{k=1}^{K-1} (l_k!)}{\left(\sum_{k=1}^{K-1} l_k + j_K - i + K - 1 \right)!} \right) \end{aligned}$$

by Lemma 1.

Substitution and cancellation yields

$$\begin{aligned} F_M(m; \lambda, K) &= e^{-\lambda} (K-1)! \sum_{j_1=0}^C \dots \sum_{j_K=0}^C \lambda^{\sum_{k=1}^K j_k} \left(\prod_{k=1}^K j_k! \right)^{-1} \\ &\quad \times s^{K-1} \sum_{i=0}^{j_K} \frac{j_K!}{i!} a_{j_K}^i s^{j_K-i} \sum_{l_1=0}^{j_1} \dots \sum_{l_{K-1}=0}^{j_{K-1}} \\ &\quad \times \prod_{k=1}^{K-1} \frac{j_k!}{(j_k - l_k)!} s^{l_k} a_{j_k}^{j_k-l_k} \frac{1}{\left(\sum_{k=1}^{K-1} l_k + j_K - i + K - 1 \right)!}, \end{aligned}$$

as desired.

[Received July 1996. Revised April 1997.]

REFERENCES

Adler, R. J. (1984), "The Supremum of a Particular Gaussian Field," *Annals of Probability*, 12, 436-444.

Alm, S. E. (1997), "On the Distributions of Scan Statistics of a Two-Dimensional Poisson Process," *Advances in Applied Probability*, 29, 1-18.

Bowyer, K. W., and Astley, S. (eds.) (1994), *State of the Art in Digital Mammographic Image Analysis: Proceedings of the 1st International Workshop on Digital Mammography, San Jose, February, 1993*, Singapore: World Scientific.

Castleman, K. R. (1996), *Digital Image Processing*, Englewood Cliffs, NJ: Prentice-Hall.

Chen, J., and Glaz, J. (1996), "Two-Dimensional Discrete Scan Statistics," *Statistics and Probability Letters*, 31, 59-68.

Cressie, N. (1977), "On Some Properties of the Scan Statistic on the Circle and the Line," *Journal of Applied Probability*, 14, 272-283.

— (1980), "The Asymptotic Distribution of the Scan Statistic under Uniformity," *Annals of Probability*, 8, 828-840.

— (1993), *Statistics for Spatial Data*, New York: Wiley.

David, H. A. (1970), *Order Statistics*, New York: Wiley.

Diggle, P. J. (1983), *Statistical Analysis of Spatial Point Patterns*, New York: Academic Press.

Doi, K., Giger, M. L., Nishikawa, R. M., and Schmidt, R. A. (eds.) (1996), *Digital Mammography '96: Proceedings of the 3rd International Workshop on Digital Mammography, Chicago, June 1996*, Amsterdam: Elsevier.

Fisher, R. A., Thornton, H. G., and Mackenzie, W. A. (1922), "The Accuracy of the Plating Method of Estimating the Density of Bacterial Populations, With Particular Reference to the Use of Thornton's Agar Medium With Soil Samples," *Annals of Applied Biology*, 9, 325-359.

Gail, A. G., Astley, S. M., Dance, A. R., and Cairns, A. Y. (eds.) (1994), *Digital Mammography: Proceedings of the 2nd International Workshop on Digital Mammography, York, England, July 1994*, Amsterdam: Elsevier.

Jacquez, G. M. (ed.) (1993), "Proceedings of the Workshop on Statistics and Computing in Disease Clustering, Port Washington, New York, 1992," *Statistics in Medicine*, 12, 1751-1968.

Jain, A. K. (1989), *Fundamentals of Digital Image Processing*, Englewood Cliffs, NJ: Prentice-Hall.

Kulldorff, M. (1997), "A Spatial Scan Statistic," *Communications in Statistics Part A—Theory and Methods*, 26, 1481-1496.

Loader, C. R. (1991), "Large-Deviation Approximations to the Distribution of Scan Statistics," *Advances in Applied Probability*, 23, 751-771.

Muise, R. R., and Smith, C. M. (1992), "Nonparametric Minefield Detection and Localization," Report CSS-TM-591-91, Naval Surface Warfare Center, Coastal Systems Station.

Naus, J. I. (1965), "Clustering of Random Points in Two Dimensions," *Biometrika*, 52, 263-267.

— (1966), "A Power Comparison of Two Tests of Non-Random Clustering," *Technometrics*, 8, 493-517.

Pyke, R. (1965), "Spacings," *Journal of the Royal Statistical Society, Ser. B*, 27, 395-436.

Serra, J. (1982), *Image Analysis and Mathematical Morphology*, London: Academic Press.

Smith, C. M. (1991), "Two-Dimensional Minefield Simulation," Report NCSC-TM-558-91, Naval Coastal Systems Center.

Vincent, L., and Soille, P. (1991), "Watersheds in Digital Spaces: An Efficient Algorithm Based on Immersion Simulations," *IEEE Transactions on Pattern Analysis and Machine Intelligence*, 13, 583-598.